Emittance growth of kicked and mismatched beams due to amplitude-dependent tune shift

E. Waagaard[†] and V. Ziemann[*]
Department of Physics and Astronomy, Uppsala University, S-75120 Uppsala, Sweden

(Received 18 March 2022; accepted 5 May 2022; published 20 May 2022)

We derive evolution equations for the first and second moments of an initially mismatched, coupled, and displaced arbitrary Gaussian phase-space distribution under the influence of decoherence due to amplitude-dependent tune shift. Moreover, we find expressions for the asymptotic values of the beam matrix and the emittance and use them to evaluate error tolerances for injection.

DOI: 10.1103/PhysRevAccelBeams.25.054001

I. INTRODUCTION

The emittance of a beam, injected into a ring, crucially depends on the initial position and angle of the injected beam as well as on the Twiss parameters of the injection line being equal to those of the ring. Once the beam is circulating in the ring, the particles perform betatron oscillations around the equilibrium orbit in the ring. Any spread of betatron frequencies, either due to chromaticity and a finite momentum spread or due to amplitude-dependent tune shift, causes the distribution of particles to distort and evolve into one with a larger emittance. This process is often referred to as decoherence. This decoherence of kicked beams due to amplitude-dependent tune shift was previously analyzed in Refs. [1–3], where, however, only the decoherence of the centroid was evaluated. Moreover, in Ref. [4], the evolution of the kicked beam matrix is calculated, and the key results are summarized in Ref. [5]. Here, we extend the analysis by considering the turn-by-turn evolution of the first and second moments of a beam that initially is both displaced and mismatched. We then follow the evolution of its first moments, which are often referred to as centroids, as well as its beam matrix and emittance, as the beam decoheres.

In order to prepare the stage for our calculations, we assume that the optics in the ring is uncoupled. We, therefore, introduce the phase shift per turn ϕ_x in the horizontal plane due to normal betatron phase advance $\mu_x = 2\pi Q_x$ and to amplitude-dependent tune shift, given by

$$\phi_x = \mu_x + \kappa_{xx}(x_1^2 + x_2^2) + \kappa_{xy}(x_3^2 + x_4^2) = \mu_x + \vec{x}^\top \bar{\kappa}_x \vec{x}, \quad (1)$$

where $\vec{x}^\top$ is the transpose of $\vec{x}$ and $\bar{\kappa}_x = \mathrm{diag}(\kappa_{xx}, \kappa_{xx}, \kappa_{xy}, \kappa_{xy})$. Here, κ_{xx} parametrizes the amplitude dependence in the horizontal plane and κ_{xy} its dependence on the amplitude in the vertical plane, also called the cross anharmonicity [6]. Here, $2J_x = x_1^2 + x_2^2 = \gamma_x x^2 + 2\alpha_x x x' + \beta_x x'^2$ with $\gamma_x = (1+\alpha_x^2)/\beta_x$ is twice the Courant-Snyder invariant J_x of the linear motion in the horizontal plane and $2J_y = x_3^2 + x_4^2 = \gamma_y y^2 + 2\alpha_y y y' + \beta_y y'^2$ in the vertical plane. We use variables $x_1, \ldots, x_4$ in normalized phase space, collectively denoted by $\vec{x} = (x_1, x_2, x_3, x_4)^\top$. They are related to the position x and angle x' by

$$\begin{pmatrix} x_1 \\ x_2 \end{pmatrix} = \mathcal{A}_x \begin{pmatrix} x \\ x' \end{pmatrix} \quad \text{with} \quad \mathcal{A}_x = \begin{pmatrix} 1/\sqrt{\beta_x} & 0 \\ \alpha_x/\sqrt{\beta_x} & \sqrt{\beta_x} \end{pmatrix}, \quad (2)$$

where α_x and β_x are the Twiss parameters in the horizontal plane of the ring at the point of injection. In most of this report, we henceforth focus on the horizontal plane. The corresponding equations for the coordinates in the other plane x_3 and x_4 the subscript x is exchanged with subscript y. Note also that, after n revolutions in the ring, the phase shift is $n\phi_x$. In passing, we point out that it is straightforward to generalize Eq. (1) to six dimensions by adding a term $\kappa_{xs}(x_5^2 + x_6^2)$, extending the definition of $\bar{\kappa}_x$ to a 6×6 matrix that includes κ_{xs} on the two lowest entries on the diagonal, and interpreting $\vec{x}$ as the corresponding six-dimensional phase-space vector. In this report, however, we focus on two and four dimensions.

We always assume that the initial beam distribution is a multivariate Gaussian. For convenience, we define it as the d-dimensional distribution

[*]Corresponding author.
volker.ziemann@physics.uu.se
[†]Present address: CERN, CH-1211 Geneva 23, Switzerland.

$$\psi_d(\vec{x};\vec{X},\sigma) = \frac{1}{(2\pi)^{d/2}\sqrt{\det\sigma}} \times \exp\left[-\frac{1}{2}\sum_{j,k=1}^{d}\sigma_{jk}^{-1}(x_j - X_j)(x_k - X_k)\right], \tag{3}$$

where d can be 2 or 4, depending on the phase space we consider. Moreover, X_j with $j = 1, \ldots, d$ are the components of the vector $\vec{X}$ with the initial centroid positions. The $d \times d$ matrix σ is the beam matrix describing the widths and orientations of the Gaussian. Note that, in coordinates of normalized phase space, the beam matrix σ of a matched beam in all planes is proportional to the unit matrix. For a matched beam, the proportionality constant in each 2×2 block on the diagonal is the emittance of the injected beam ε_0 in the respective plane. Throughout this report, we normalize positions and beam sizes by $\sqrt{\varepsilon_0}$, such that all numerical values are given in units of the corresponding rms values of the beam size or the angular divergence. For example, the physical position x is related to x_1 through $x_1 = x/\sqrt{\beta}$ and normalized by $\sqrt{\varepsilon_0}$ to $x/\sqrt{\varepsilon_0\beta}$.

In the following sections, we first follow the centroid of this Gaussian as it decoheres, where we assume that σ is an arbitrary beam matrix, not necessarily matched to the ring into which we assume the beam is injected. In Sec. III, we show that our general result reproduces the results from Ref. [1] for a matched injected beam. In the following sections, we calculate the turn-by-turn evolution of the second moments, in general, before considering a matched beam and an arbitrary beam matrix in one transverse plane. In Sec. VII, we consider injection of a transversely coupled beam matrix. In all cases, we derive expressions for the asymptotic beam matrix and then use them to determine error tolerances. In separate sections, we discuss the asymptotic emittance growth due to a mismatched dispersion and indicate how to include decoherence due to chromaticity into our framework before summarizing our results in the conclusions.

II. CENTROID

We now calculate the betatron motion with phase advance μ_x of the centroid of a Gaussian and denote the centroid position in the horizontal plane after n turns by $\hat{X}_1$ and $\hat{X}_2$, which leads us to

$$\hat{X}_1 + i\hat{X}_2 = e^{-in\mu_x}\langle e^{-in\vec{x}^\top\bar{\kappa}_x\vec{x}}(x_1 + ix_2)\rangle, \tag{4}$$

where the angle brackets denote averaging over the initial Gaussian distribution from Eq. (3). We point out that damping can be taken into account by adding a factor e^{-n/N_d} (with damping time given in number of turns N_d) to the right-hand side of Eq. (4). But in this report we do not pursue this further. Since we will encounter similar integrals to those appearing in Eq. (4) along the way, we introduce the notation

$$I[n,p] = \langle e^{-in\vec{x}^\top\bar{\kappa}_x\vec{x}}p(\vec{x})\rangle, \tag{5}$$

where $p(\vec{x})$ is a multivariate polynomial in the phase-space coordinates $x_1, \ldots, x_d$. In Eq. (4), for example, we have $p(\vec{x}) = x_1 + ix_2$. Moreover, Eq. (4) can also be expressed as $\hat{X}_1 + iX_2 = e^{-in\mu_x}I[n, x_1 + ix_2]$.

In the next step, we evaluate $I[n,p]$ by explicitly writing it as a Gaussian integral:

$$I[n,p] = \frac{1}{(2\pi)^{d/2}\sqrt{\det\,\sigma}}\int d^d x e^{-(1/2)\sum_{j,k=1}^{d}\sigma_{jk}^{-1}(x_j-X_j)(x_k-X_k)}e^{-in\vec{x}^\top\bar{\kappa}_x\vec{x}}, \tag{6}$$

where, for brevity, we suppress the limits of the integrals, which always extend from $-\infty$ to ∞. We simplify the integrand by expressing x_1^2 as

$$x_1^2 = (x_1 - X_1)^2 + 2X_1x_1 - X_1^2 = (x_1 - X_1)^2 + 2X_1(x_1 - X_1) + X_1^2 \tag{7}$$

and likewise for $x_2^2, \ldots, x_d^2$. Inserting in Eq. (6) and combining terms, we arrive at

$$I[n,p] = \frac{e^{-in\vec{X}^\top\bar{\kappa}_x\vec{X}}}{(2\pi)^{d/2}\sqrt{\det\,\sigma}}\int d^d x e^{-(1/2)\sum_{j,k=1}^{d}[\sigma_{jk}^{-1}+2in(\bar{\kappa}_x)_{kj}](x_j-X_j)(x_k-X_k)}e^{-2in\vec{X}^\top\bar{\kappa}_x(\vec{x}-\vec{X})}p(\vec{x}). \tag{8}$$

We now introduce the abbreviations

$$A_{jk} = \sigma_{jk}^{-1} + 2in(\bar{\kappa}_x)_{jk} \quad \text{and} \quad B_j = 2n\sum_{k=1}^{d}(\bar{\kappa}_x)_{jk}X_k. \tag{9}$$

The substitution $\vec{y} = \vec{x} - \vec{X}$ then allows us to write Eq. (8) as

$$I[n,p] = \frac{e^{-in\vec{X}^\top \bar{\kappa}_x \vec{X}}}{(2\pi)^{d/2}\sqrt{\det \sigma}} \int d^d y e^{-(1/2)\sum_{j,k=1}^d A_{jk} y_j y_k - i\sum_{j=1}^d B_j y_j} p(\vec{y} + \vec{X}). \tag{10}$$

In the final step, we find a substitution that helps us to remove the term that is linear in y_j in the exponent. We, therefore, introduce a further substitution $z_j = y_j + h_j$ and find h_j that removes that term. We insert this substitution into the exponent and obtain

$$\begin{aligned} &-\frac{1}{2}\sum_{j,k=1}^d A_{jk}(z_j - h_j)(z_k - h_k) - i\sum_{j=1}^d B_j(z_j - h_j) \\ &\quad = -\frac{1}{2}\sum_{j,k=1}^d A_{jk} z_j z_k + i\sum_{j=1}^d B_j h_j - \frac{1}{2}\sum_{j,k=1}^d A_{jk} h_j h_k + \sum_{j=1}^d \left[\frac{1}{2}\sum_{k=1}^d 2A_{jk} h_k - iB_j\right] z_j \end{aligned} \tag{11}$$

which implies that

$$h_k = i\sum_{j=1}^d A_{kj}^{-1} B_j \tag{12}$$

makes the square bracket zero and, thus, removes the linear term. After substituting h_k into the right-hand side of Eq. (11), the exponent assumes the form

$$-\frac{1}{2}\vec{B}^\top A^{-1}\vec{B} - \frac{1}{2}\sum_{j,k=1}^d A_{jk} z_j z_k. \tag{13}$$

For $I[n,p]$, we find

$$\begin{aligned} I[n,p] &= \frac{e^{-in\vec{X}^\top \bar{\kappa}_x \vec{X} - (1/2)\vec{B}^\top A^{-1}\vec{B}}}{(2\pi)^{d/2}\sqrt{\det \sigma}} \int d^d z e^{-(1/2)\sum_{j,k=1}^d A_{jk} z_j z_k} p(\vec{x}) \\ &= \frac{e^{-in\vec{X}^\top \bar{\kappa}_x \vec{X} - 2n^2 \vec{X}^\top \bar{\kappa}_x (\mathbf{1} + 2in\sigma\bar{\kappa}_x)^{-1}\sigma\bar{\kappa}_x \vec{X}}}{(2\pi)^{d/2}\sqrt{\det \sigma}} \int d^d z e^{-(1/2)\sum_{j,k=1}^d A_{jk} z_j z_k} p(\vec{x}) \end{aligned} \tag{14}$$

with

$$\vec{x} = \vec{z} + \vec{X} - iA^{-1}\vec{B} = \vec{z} + \vec{Y} \quad \text{and} \quad \vec{Y} = (\mathbf{1} - 2inA^{-1}\bar{\kappa}_x)\vec{X}. \tag{15}$$

Moreover, we use the definitions of A and $\vec{B}$ from Eq. (9) to obtain

$$A^{-1}\vec{B} = 2n(\mathbf{1} + 2in\sigma\bar{\kappa}_x)^{-1}\sigma\bar{\kappa}_x \vec{X} \quad \text{and} \quad \vec{Y} = (\mathbf{1} + 2in\sigma\bar{\kappa}_x)^{-1}\vec{X}. \tag{16}$$

The integrals are evaluated with the help of the identities [7]

$$\begin{aligned} \int d^d z e^{-(1/2)\sum_{j,k=1}^d A_{jk} z_j z_k} &= \frac{(2\pi)^{d/2}}{\sqrt{\det A}}, \\ \int d^d z e^{-(1/2)\sum_{j,k=1}^d A_{jk} z_j z_k} z_m &= 0, \\ \int d^d z e^{-(1/2)\sum_{j,k=1}^d A_{jk} z_j z_k} z_m z_n &= \frac{(2\pi)^{d/2}}{\sqrt{\det A}} A_{mn}^{-1}, \end{aligned} \tag{17}$$

which follow from the well-known identities for normalizing a Gaussian distribution and how the first and second moments are given in terms of the covariance matrix. In particular, the centroid positions after n turns $\hat{X}_1 + i\hat{X}_2$, identified by a caret, turn out to be

$$\begin{aligned}\hat{X}_1 + i\hat{X}_2 &= e^{-in\mu_x} \frac{e^{-in\vec{X}^\top \bar{\kappa}_x \vec{X} - (1/2)\vec{B}^\top A^{-1}\vec{B}}}{(2\pi)^{d/2}\sqrt{\det\sigma}} \frac{(2\pi)^{d/2}}{\sqrt{\det A}}(Y_1 + iY_2) \\ &= \frac{e^{-in\mu_x - in\vec{X}^\top \bar{\kappa}_x \vec{X} - 2n^2 \vec{X}^\top \bar{\kappa}_x (\mathbf{1} + 2in\sigma\bar{\kappa}_x)^{-1}\sigma\bar{\kappa}_x \vec{X}}}{\sqrt{\det(\mathbf{1} + 2in\sigma\bar{\kappa}_x)}}(Y_1 + iY_2), \end{aligned} \tag{18}$$

where $\vec{Y}$ is defined in Eq. (16). We point out that the result in Eq. (18) is valid for dimensions $d = 2$ or 4 and for arbitrary beam matrices σ, including matched beams. In order to compare with the results from Ref. [1], we consider such a matched beam for $d = 2$ in the following section.

III. AMPLITUDE DEPENDENCE

In order to obtain some intuition, we compare our calculation with Ref. [1] and set $d = 2$ and $\kappa_{xx} = \kappa$ before calculating the evolution of the oscillation amplitude of the centroid a_n with the number of turns n:

$$a_n = \sqrt{|\hat{\vec{X}}|^2} = \sqrt{\hat{X}_1^2 + \hat{X}_2^2} = \sqrt{(\hat{X}_1 + i\hat{X}_2)(\hat{X}_1 - i\hat{X}_2)} \tag{19}$$

for a matched beam with the 2×2 beam matrix

$$\sigma = \varepsilon_0 \mathbf{1}. \tag{20}$$

To do so, we take the squared modulus of Eq. (18) and consider one term at a time. First, we consider $\vec{Y}$ and calculate $|\vec{Y}|^2$ from Eq. (16), which leads to

$$\begin{aligned}|\vec{Y}|^2 &= \left(\frac{1}{1 + 2in\kappa\varepsilon_0}\right)\left(\frac{1}{1 - 2in\kappa\varepsilon_0}\right)|\vec{X}|^2 \\ &= \frac{1}{1 + 4n^2\kappa^2\varepsilon_0^2}|\vec{X}|^2. \end{aligned} \tag{21}$$

Second, we consider the root in the denominator of Eq. (18), which simplifies to

$$\sqrt{\det(\mathbf{1} + 2in\kappa\sigma)} = \sqrt{\det[(1 + 2in\kappa\varepsilon_0)\mathbf{1}]} = 1 + 2in\kappa\varepsilon_0, \tag{22}$$

which has squared modulus $1 + 4n^2\kappa^2\varepsilon_0^2$ that consequently also appears in the denominator. Finally, the third term in the exponent of Eq. (18) simplifies to

$$\begin{aligned}\vec{X}^\top(\mathbf{1} + 2in\kappa\sigma)^{-1}\sigma\vec{X} &= \vec{X}^\top \frac{\varepsilon_0}{1 + 2in\kappa\varepsilon_0}\vec{X} \\ &= \frac{\varepsilon_0|\vec{X}|^2}{1 + 4n^2\kappa^2\varepsilon_0^2}(1 - 2in\kappa\varepsilon_0). \end{aligned} \tag{23}$$

Since the imaginary part in the exponent has unit modulus, only the real part appears in the modulus of the whole expression. Inserting the three contributions into Eq. (18) results in

$$|\hat{\vec{X}}|^2 = \frac{|\vec{X}|^2}{(1 + 4n^2\kappa^2\varepsilon_0^2)^2} \exp\left[-\frac{4n^2\kappa^2\varepsilon_0|\vec{X}|^2}{1 + 4n^2\kappa^2\varepsilon_0^2}\right]. \tag{24}$$

Expressing this equation in terms of the amplitude a_n with the initial amplitude $a_0 = \sqrt{|\vec{X}|^2}$, we find

$$a_n = \frac{a_0}{1 + 4n^2\kappa^2\varepsilon_0^2} \exp\left[-\frac{a_0^2}{2\varepsilon_0}\frac{4n^2\kappa^2\varepsilon_0^2}{1 + 4n^2\kappa^2\varepsilon_0^2}\right], \tag{25}$$

which agrees with the result for the amplitude decoherence from Ref. [1] provided we identify $\theta = 2n\kappa\varepsilon_0$ and $\varepsilon_0 = 1$.

In Fig. 1, we use Eq. (25) to show the dependence of the amplitude a_n on the number of turns for starting amplitudes $a_0 = \varepsilon_0$ and $a_0 = 2\varepsilon_0$. We observe that the initial reduction of the amplitude follows a Gaussian behavior, whereas for large n the exponential approaches $e^{-a_0^2/2\varepsilon_0}$ and the turn evolution is governed by the factor $1 + 4n^2\kappa^2\varepsilon_0^2$ in the denominator. The transition between the two regimes, already discussed in Ref. [1], appears around $\theta \approx 1$ when $n \approx 1/2\kappa\varepsilon_0$. A larger starting amplitude $a_0 = 2$ (red dashed curve) leads to a faster initial reduction of the amplitude to

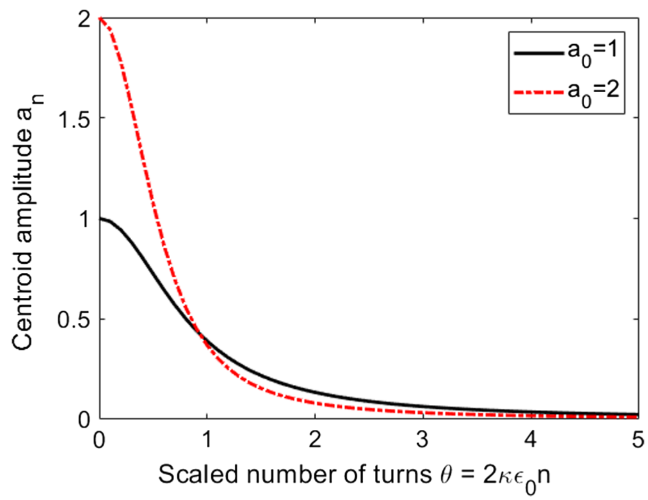

FIG. 1. Amplitude of the beam centroid (in units of $\sqrt{\varepsilon_0}$) versus the turn number n, parametrized as $\theta = 2\kappa\varepsilon_0 n$ with parameters $\varepsilon_0 = 1$ and $\kappa = 0.1$ and for two values $a_0 = 1$ and $a_0 = 2$ of the initial displacement.

values below those for $a_0 = 1$ (black solid curve). Note that the curves cross near the transition at $\theta \approx 1$.

In the next section, we turn to the evolution of the beam matrix and the emittance.

IV. BEAM MATRIX AND EMITTANCE

In this section, we consider the general case with d dimensions. The beam size after n turns is related to the second moments of the distribution after n turns, again identified by a caret. One of the moments $\langle \hat{x}_1^2 \rangle$ is given by

$$\langle \hat{x}_1^2 \rangle = \langle (x_1 \cos n\phi_x + x_2 \sin n\phi_x)^2 \rangle. \tag{26}$$

The angle brackets denote averaging over the initial distribution from Eq. (3) in d dimensions and ϕ_x is defined in Eq. (1). All other moments, such as $\langle \hat{x}_1 \hat{x}_2 \rangle$ and $\langle \hat{x}_2^2 \rangle$, are given by similar equations. We now express the trigonometric functions by their exponential representation and arrive at

$$\langle \hat{x}_1^2 \rangle = \frac{1}{4} \langle (2 + e^{2in\phi_x} + e^{-2in\phi_x}) x_1^2 - 2i(e^{2in\phi_x} - e^{-2in\phi_x}) x_1 x_2 + (2 - e^{2in\phi_x} - e^{-2in\phi_x}) x_2^2 \rangle. \tag{27}$$

At this point, we note that only expressions of the type $e^{-im\phi}$ with $m = 0$, $2n$, and $-2n$ appear. We, therefore, introduce

$$J[m, p; \mu_x, \bar{\kappa}_x] = \langle e^{-im\phi_x} p(\vec{x}) \rangle = \langle e^{-im\mu_x - im\vec{x}^\top \bar{\kappa}_x \vec{x}} p(\vec{x}) \rangle, \tag{28}$$

where $p(\vec{x})$ is one of x_1^2, $x_1 x_2$, or x_2^2. For brevity, we omit the arguments after the semicolon if they are unambiguous and just write $J[m, p]$. In the next step, we use Eq. (28) to rewrite $\langle \hat{x}_1^2 \rangle$ in Eq. (27), which leads us to

$$\begin{aligned}
\langle \hat{x}_1^2 \rangle &= \frac{1}{4} (2J[0, x_1^2] + J[-2n, x_1^2] + J[2n, x_1^2] - 2iJ[-2n, x_1 x_2] + 2iJ[2n, x_1 x_2] \\
&\quad + 2J[0, x_2^2] - J[-2n, x_2^2] - J[2n, x_2^2]) \\
&= \frac{1}{2} \{ J[0, x_1^2] + \mathrm{Re}(J[-2n, x_1^2]) \} + \mathrm{Im}(J[-2n, x_1 x_2]) + \frac{1}{2} \{ J[0, x_2^2] - \mathrm{Re}(J[-2n, x_2^2]) \},
\end{aligned} \tag{29}$$

where we use

$$J[-m, p] + J[m, p] = 2\mathrm{Re}(J[-m, p]) \quad \text{and} \quad J[-m, p] - J[m, p] = 2i\mathrm{Im}(J[-m, p]). \tag{30}$$

The corresponding expressions for $\langle \hat{x}_1 \hat{x}_2 \rangle$, $\langle \hat{x}_2^2 \rangle$, and $\langle \hat{x}_1 \hat{x}_3 \rangle$ can be found in the Appendix.

In order to evaluate $J[m, p]$, we note that it is closely related to $I[m, p]$ from Eq. (6), which allows us to express $J[m, p]$ as

$$J[m, p] = e^{-im\mu_x} \langle e^{-im\vec{x}^\top \bar{\kappa}_x \vec{x}} p(\vec{x}) \rangle = e^{-im\mu_x} I[m, p]. \tag{31}$$

This leaves us the task to evaluate $I[m, p]$ for $p = x_r x_s$, where r and s assume values between 1 and d. Expressing x_r through $x_r = z_r + Y_r$ and inserting this in Eq. (14), we obtain

$$\begin{aligned}
I[m, x_r x_s] &= \frac{e^{\psi(m)}}{(2\pi)^{d/2} \sqrt{\det \sigma}} \int d^d z e^{-(1/2) \sum_{j,k=1}^{d} A_{jk} z_j z_k} (z_r + Y_r)(z_s + Y_s) \\
&= \frac{e^{\psi(m)}}{(2\pi)^{d/2} \sqrt{\det \sigma}} \int d^d z e^{-(1/2) \sum_{j,k=1}^{d} A_{jk} z_j z_k} (z_r z_s + z_r Y_s + z_s Y_r + Y_r Y_s)
\end{aligned} \tag{32}$$

with the abbreviation

$$\psi(m) = -im\vec{X}^\top \bar{\kappa}_x \vec{X} - 2m^2 \vec{X}^\top \bar{\kappa}_x (\mathbf{1} + 2im\sigma\bar{\kappa}_x)^{-1} \sigma \bar{\kappa}_x \vec{X}. \tag{33}$$

The four terms inside the integral are evaluated by using the expressions from Eq. (17), and this leads to

$$I[m,x_rx_s] = \frac{e^{\psi(m)}}{(2\pi)^{d/2}\sqrt{\det\sigma}}\frac{(2\pi)^{d/2}}{\sqrt{\det A}}(A_{rs}^{-1} + Y_rY_s) = \frac{e^{\psi(m)}}{\sqrt{\det(\mathbf{1}+2im\sigma\bar{\kappa}_x)}}(A_{rs}^{-1} + Y_rY_s), \tag{34}$$

and for $J[m,x_rx_s]$ we obtain with Eq. (31)

$$J[m,x_rx_s] = \frac{e^{-im\mu_x+\psi(m)}}{\sqrt{\det(\mathbf{1}+2im\sigma\bar{\kappa}_x)}}(A_{rs}^{-1} + Y_rY_s) \tag{35}$$

with $A^{-1} = (\mathbf{1}+2im\sigma\bar{\kappa}_x)^{-1}\sigma$ and $\vec{Y} = (\mathbf{1}+2im\sigma\bar{\kappa}_x)^{-1}\vec{X}$.

The matrix elements of the beam matrix after n turns $\hat{\sigma}_{rs}$ are related to the second moments $\langle\hat{x}_r\hat{x}_s\rangle$ via

$$\hat{\sigma}_{rs} = \langle(\hat{x}_r - \hat{X}_r)(\hat{x}_s - \hat{X}_s)\rangle = \langle\hat{x}_r\hat{x}_s\rangle - \hat{X}_r\hat{X}_s, \tag{36}$$

which requires us also to subtract $\hat{X}_r\hat{X}_s$ from the second moments, for which we resort to Eq. (18) to calculate $\hat{X}_1$ and $\hat{X}_2$. Both the second moments and the centroids must be calculated for the same number of turns n. These equations are valid for any mismatched and transversely coupled beam that additionally is injected off axis with $\vec{X} \neq 0$.

V. EMITTANCE GROWTH FOR A MATCHED BEAM

Just as we did for the amplitude decoherence, we now consider $d = 2$, set $\kappa_{xx} = \kappa$, and evaluate the turn-by-turn evolution of the second moments and the emittance for a matched beam with $\sigma = \varepsilon_0\mathbf{1}$, analogous to the analysis from Ref. [4]. We start our analysis by evaluating the terms that enter $J[m,x_rx_s]$. The first is

$$(\mathbf{1}+2im\kappa\sigma)^{-1} = \frac{1}{1+2im\kappa\varepsilon_0}\mathbf{1}, \tag{37}$$

which leads us to

$$\vec{Y} = (\mathbf{1}+2im\kappa\sigma)^{-1}\vec{X} = \frac{1}{1+2im\kappa\varepsilon_0}\vec{X} \tag{38}$$

and

$$A^{-1} = (\mathbf{1}+2im\kappa\sigma)^{-1}\sigma = \frac{\varepsilon_0}{1+2im\kappa\varepsilon_0}\mathbf{1}. \tag{39}$$

The root in the denominator of Eq. (35) simplifies to

$$\sqrt{\det(\mathbf{1}+2im\kappa\sigma)} = 1+2im\kappa\varepsilon_0, \tag{40}$$

and $\psi(m)$ from Eq. (33) becomes

$$\begin{aligned}\psi(m) &= -im\kappa(X_1^2+X_2^2) - 2m^2\kappa^2\vec{X}^\top\frac{\varepsilon_0}{1+2im\kappa\varepsilon_0}\vec{X} \\ &= -im\kappa|\vec{X}|^2 - 2m^2\kappa^2\frac{\varepsilon_0}{1+2im\kappa\varepsilon_0}|\vec{X}|^2 \\ &= -\frac{im\kappa}{1+2im\kappa\varepsilon_0}|\vec{X}|^2.\end{aligned} \tag{41}$$

Inserting these expressions into Eq. (35), we find

$$\begin{aligned}J[m,x_rx_s] &= \frac{e^{-im\mu_x-[im\kappa/(1+2im\kappa\varepsilon_0)]|\vec{X}|^2}}{1+2im\kappa\varepsilon_0} \times\left(\frac{\varepsilon_0}{1+2im\kappa\varepsilon_0}\delta_{rs} + \frac{X_rX_s}{(1+2im\kappa\varepsilon_0)^2}\right) \\ &= \frac{e^{-im\mu_x-[im\kappa/(1+2im\kappa\varepsilon_0)]|\vec{X}|^2}}{(1+2im\kappa\varepsilon_0)^2}\left(\varepsilon_0\delta_{rs} + \frac{X_rX_s}{1+2im\kappa\varepsilon_0}\right)\end{aligned} \tag{42}$$

that we use to calculate the second moments from Eqs. (29) and (A2).

For the beam matrix, we also need the centroid motion that we previously analyzed in Sec. II and for a matched beam in Sec. III. Adapting Eq. (18) to $\sigma = \varepsilon_0\mathbf{1}$, we arrive at

$$\hat{X}_1 + i\hat{X}_2 = \frac{e^{-in\mu_x-[in\kappa/(1+2in\kappa\varepsilon_0)]|\vec{X}|^2}}{(1+2in\kappa\varepsilon_0)^2}(X_1+iX_2), \tag{43}$$

whose modulus again leads to Eq. (24). We emphasize that here n is the number of turns and not a general parameter such as m in Eq. (42).

From the second moments from Eq. (A2), together with $J[m,x_rx_s]$ from Eq. (42) and the centroid from Eq. (43), we prepared a MATLAB [8] script, available from Ref. [9], to follow the centroids $\vec{X}$, the beam matrix $\hat{\sigma}$ from Eq. (36), and the emittance $\hat{\varepsilon} = \sqrt{\det\hat{\sigma}}$ for a number of turns. Figure 2 shows $\hat{X}_1$ (top), $\hat{\sigma}_{11}$ and $\hat{\sigma}_{12}$ (middle), and the emittance $\hat{\varepsilon}$ (bottom) as a function of n. The parameters in this simulation, chosen to illustrate the dynamics, are $\mu_x/2\pi = 0.028$, $\kappa = 0.001$, and $\varepsilon_0 = 1$. Initially, the beam is offset by $X_1 = 2$, and the top plot shows oscillations that initially follow a Gaussian behavior before later decaying at a much slower rate, as discussed in Sec. III. At the same time, the beam size $\hat{\sigma}_{11}$ oscillates at twice the frequency of the centroid and increases toward a higher level. Intermittently, the correlation $\hat{\sigma}_{12}$ increases, which is due to distortions of the initially matched beam while it decoheres. Toward the end of the simulation, $\hat{\sigma}_{12}$ decreases to zero, because the beam decoheres and reaches its equilibrium configuration. The bottom plot shows the emittance $\hat{\varepsilon}$, which has tripled compared to the initially injected beam.

The equilibrium value that is reached after the decoherence has finished is easily calculated by realizing

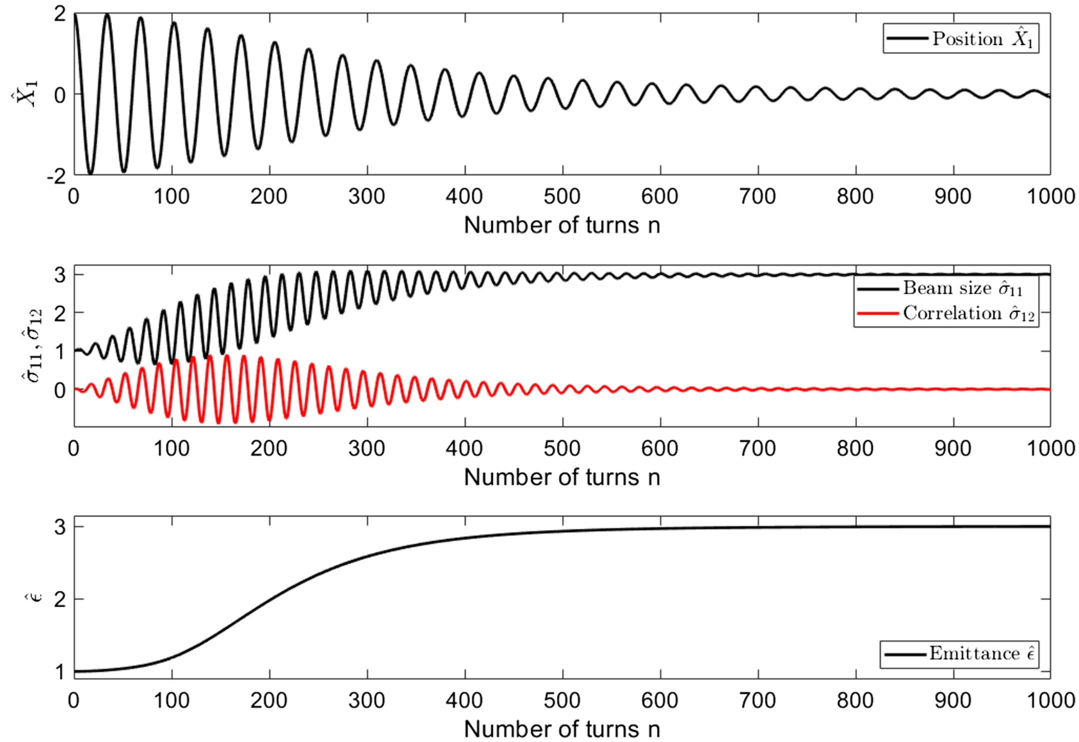

FIG. 2. The centroid X_1 (top), the beam matrix elements σ_{11} and σ_{12} (middle), and the emittance (bottom) as a function of the turn number n for a matched beam that is injected with initial offset $X_1 = 2$. The parameters used are $\mu/2\pi = 0.028$ and $\kappa\varepsilon_0 = 0.001$. The vertical axes are normalized to appropriate powers of ε_0.

that the centroids $\hat{\vec{X}}$ as well as the coefficients $J[m, x_r x_s]$ vanish for large values of $m = -2n$. Therefore, only terms with $J[0, x_r x_s]$ that appear in Eq. (A2) survive in this limit. This leads to

$$\begin{aligned}\langle\hat{x}_1^2\rangle &= \frac{1}{2}(J[0,x_1^2] + J[0,x_2^2]) = \varepsilon_0 + \frac{1}{2}(X_1^2 + X_2^2),\\ \langle\hat{x}_1\hat{x}_2\rangle &= 0,\\ \langle\hat{x}_2^2\rangle &= \frac{1}{2}(J[0,x_1^2] + J[0,x_2^2]) = \varepsilon_0 + \frac{1}{2}(X_1^2 + X_2^2),\end{aligned} \quad (44)$$

where using Eq. (42) for $m = 0$ gives us $J[0, x_r, x_2] = (\varepsilon_0\delta_{rs} + X_r X_s)$ and the asymptotic emittance $\hat{\varepsilon} = \sqrt{\langle\hat{x}_1^2\rangle\langle\hat{x}_2^2\rangle - \langle\hat{x}_1\hat{x}_2\rangle^2}$. The asymptotic emittance growth then becomes $\hat{\varepsilon} - \varepsilon_0 = (X_1^2 + X_2^2)/2$, which is the Courant-Snyder invariant, written in coordinates of normalized phase space. Expressed through physical coordinates, the centroid position X and angle X', the emittance growth becomes

$$\hat{\varepsilon} - \varepsilon_0 = \frac{1}{2}(\gamma_x X^2 + 2\alpha_x X X' + \beta_x X'^2). \quad (45)$$

This is not really a surprise, because the amplitude-dependent tune shift does not change the oscillation amplitudes of individual particles, such that the asymptotic emittance growth agrees with the value caused by decoherence (Sec. 8.2 in Ref. [10]) due to chromaticity and momentum spread; only the transient behavior of the two processes differs.

VI. MISMATCHED BEAM

In this section, we explore the decoherence in one plane ($d = 2$) of a mismatched beam that is injected on axis ($\vec{X} = 0$) into the ring. In this case, $\vec{Y} = 0$ and $\psi(m) = 0$ from Eq. (33), which causes $J[m, x_r x_s]$ to simplify to

$$J[m, x_r x_s] = \frac{1}{\sqrt{\det(\mathbf{1} + 2im\kappa\sigma)}}(\mathbf{1} + 2im\kappa\sigma)^{-1}\sigma. \quad (46)$$

Moreover, we have $\hat{\vec{X}} = 0$. This makes calculating the beam matrix $\hat{\sigma}$ and the emittance $\hat{\varepsilon}$ straightforward. Figure 3 shows the result in position $\hat{X}_1$ (top), sigma matrix elements $\hat{\sigma}_{11}$ and $\hat{\sigma}_{12}$ (middle), and the emittance $\hat{\varepsilon}$ (bottom) for an injected beam that has initial emittance unity. We assume $\alpha = 0$ but significantly increase the beta function to twice the value of the matched beam. All other parameters are equal to those already used in Fig. 2. We see that the beam size $\hat{\sigma}_{11}$ and correlation $\hat{\sigma}_{12}$ oscillate, but this motion slowly decoheres and reaches a new equilibrium value. At the same time, the emittance increases and also settles toward a new, and larger, equilibrium value.

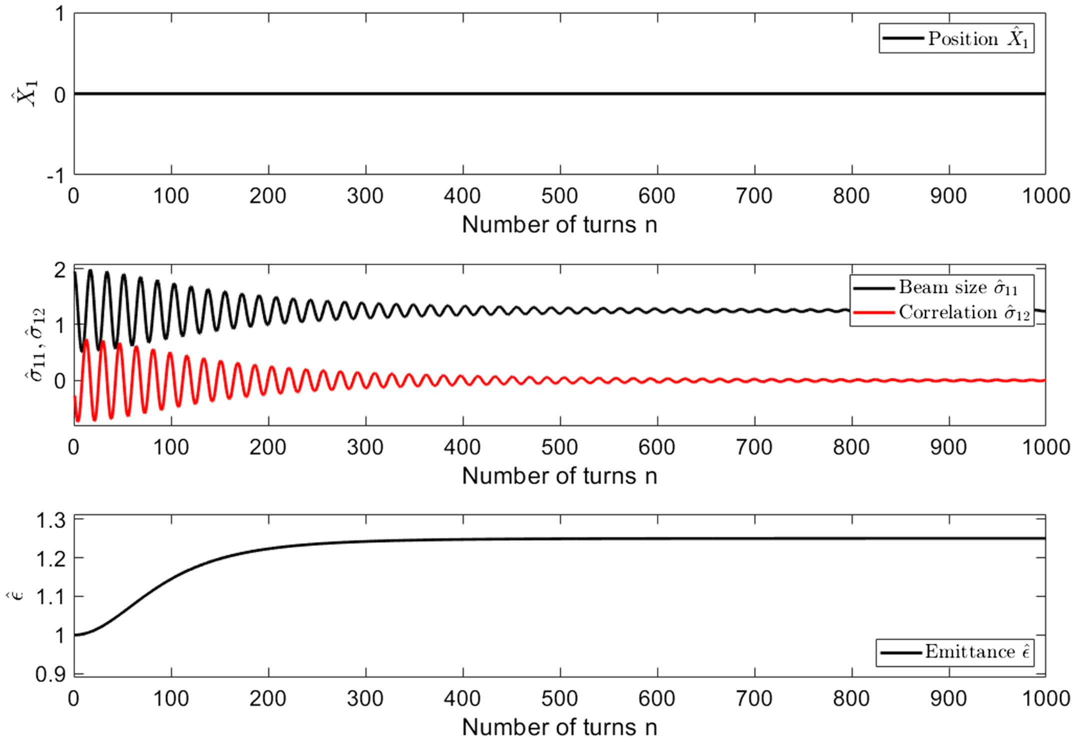

FIG. 3. The parameters $\hat{X}_1$, $\hat{\sigma}_{11}$, and $\hat{\sigma}_{12}$ and emittance as a function of the turn number n for a beam that is injected on axis but with a beta function β_0 that is twice the matched value β. All other parameters are equal to those used in Fig. 2. The vertical axes are normalized to appropriate powers of ε_0.

Figure 4 shows a simulation with parameters used in Fig. 3, only the initial value of X_2 is set to $X_2 = 1$. We see that $\hat{X}_1$ (top panel) performs betatron oscillation with slowly decreasing amplitude, which motivates the increased range of turns shown. Qualitatively, $\hat{\sigma}_{11}$ and $\hat{\sigma}_{12}$ (middle) show similar behavior to that in Fig. 3. Likewise, the emittance (bottom) increases to a new equilibrium value that is, however, larger than the one in Fig. 3 due to the nonzero value of X_2.

These new equilibrium values are easily calculated from Eqs. (29) and (A2). As before, realizing that all $J[m, x_r x_s]$ asymptotically vanish, this leaves us with

$$\begin{aligned}\langle\hat{x}_1^2\rangle &= \frac{1}{2}(J[0,x_1^2]+J[0,x_2^2]) = \frac{1}{2}(\sigma_{11}+\sigma_{22})+\frac{1}{2}(X_1^2+X_2^2),\\ \langle\hat{x}_1\hat{x}_2\rangle &= 0,\\ \langle\hat{x}_2^2\rangle &= \frac{1}{2}(J[0,x_1^2]+J[0,x_2^2]) = \frac{1}{2}(\sigma_{11}+\sigma_{22})+\frac{1}{2}(X_1^2+X_2^2),\end{aligned} \tag{47}$$

which is valid even for nonzero initial displacement $\vec{X}$. Here, $(X_1^2+X_2^2)/2$ is again the Courant-Snyder invariant of the centroid. Moreover, σ_{jk} is the beam matrix of the injected beam in normalized coordinates, which is related to the beam matrix in physical coordinates $\tilde{\sigma}$ by

$$\begin{pmatrix}\sigma_{11} & \sigma_{12}\\ \sigma_{12} & \sigma_{22}\end{pmatrix} = \mathcal{A}_x\tilde{\sigma}\mathcal{A}_x^\top \quad \text{with} \quad \tilde{\sigma} = \varepsilon_0\begin{pmatrix}\beta_0 & -\alpha_0\\ -\alpha_0 & \gamma_0\end{pmatrix}, \tag{48}$$

where ε_0 is the emittance and of the injected beam, α_0, β_0, and γ_0 are its Twiss parameters, and $\mathcal{A}_x$ is defined in Eq. (2). Evaluating this expression and calculating $(\sigma_{11}+\sigma_{22})/2$, we arrive at

$$\frac{1}{2}(\sigma_{11}+\sigma_{22}) = \varepsilon_0 B_{mag} \quad \text{with}$$
$$B_{mag} = \frac{1}{2}\left[\left(\frac{\beta_0}{\beta_x}+\frac{\beta_x}{\beta_0}\right)+\beta_x\beta_0\left(\frac{\alpha_x}{\beta_x}-\frac{\alpha_0}{\beta_0}\right)^2\right], \tag{49}$$

where we see that B_{mag} is the factor by which the emittance of the injected beam is asymptotically increased by decoherence after injecting a mismatched beam. Summarily, we find that the asymptotic emittance due to a displaced injected centroid and mismatched beam matrix becomes

$$\hat{\varepsilon} = \varepsilon_0 B_{mag} + \frac{1}{2}(\gamma_x X^2 + 2\alpha_x XX' + \beta_x X'^2) \tag{50}$$

with B_{mag} defined in Eq. (49) and the Twiss parameters of the ring α_x, β_x, and γ_x. On-axis injection with the ratio of $\beta_0/\beta_x = 2$ and $\alpha = \alpha_0 = 0$, which is used in the simulation

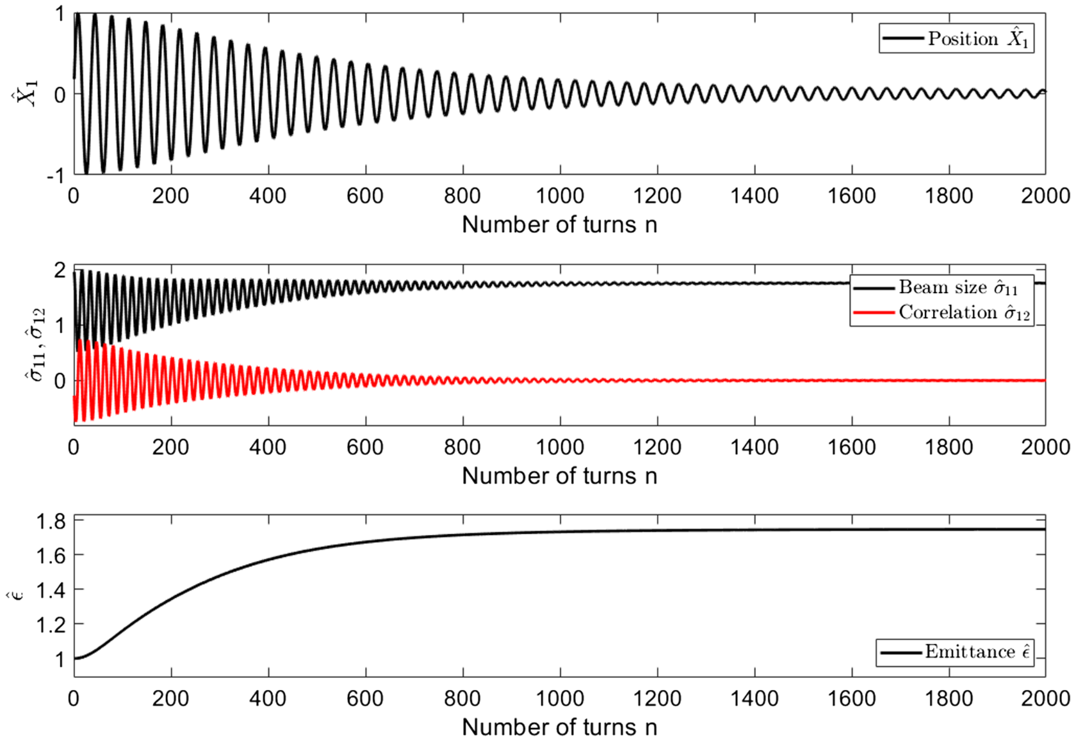

FIG. 4. The same parameters that are shown in Fig. 3 but with an additional steering error at injection $X_2 = 1$. The slow decrease of $\hat{X}_1$ motivates the extended range of turns.

shown in Fig. 3, leads to $B_{mag} = 1.25$, which agrees with the observed emittance growth visible in the bottom panel. Likewise, additionally setting $X_2 = 1$ increases the emittance to $\hat{\varepsilon} = B_{mag}\varepsilon_0 + X_2^2/2 = 1.75\varepsilon_0$, which agrees with the final value shown in the bottom panel in Fig. 4.

VII. TRANSVERSE COUPLING

For $d = 4$, Eq. (36), with $J[m, x_r, x_s]$ defined in Eq. (35), describes the dynamics of a 4×4 coupled beam matrix $\tilde{\sigma}$ that is injected into a ring. In order to analyze it in a systematic way, we base our description on the parametrization of coupled transfer matrices from Refs. [11,12] and write $\tilde{\sigma}$ as

$$\tilde{\sigma} = T^{-1}\tilde{\mathcal{A}}^{-1}\bar{\varepsilon}(\tilde{\mathcal{A}}^{-1})^\top (T^{-1})^\top \quad \text{with}$$

$$\tilde{\mathcal{A}} = \begin{pmatrix} \tilde{\mathcal{A}}_a & 0 \\ 0 & \tilde{\mathcal{A}}_b \end{pmatrix} \quad \text{and} \quad \tilde{\mathcal{A}}_a = \begin{pmatrix} \frac{1}{\sqrt{\beta_a}} & 0 \\ \frac{\alpha_a}{\sqrt{\beta_a}} & \sqrt{\beta_a} \end{pmatrix}, \tag{51}$$

where $\tilde{\mathcal{A}}_b$ is defined analogously. Moreover, $\bar{\varepsilon} = \mathrm{diag}(\varepsilon_a, \varepsilon_a, \varepsilon_b, \varepsilon_b)$ contains the emittances of two eigenmodes. T and its inverse T^{-1} describe transverse coupling and are given by

$$T = \begin{pmatrix} g\mathbf{1} & -C \\ C^+ & g\mathbf{1} \end{pmatrix} \quad \text{and} \quad T^{-1} = \begin{pmatrix} g\mathbf{1} & C \\ -C^+ & g\mathbf{1} \end{pmatrix}, \tag{52}$$

with the 2×2 identity matrix $\mathbf{1}$, the 2×2 coupling matrix C, its symplectic conjugate $C^+ = C^{-1} \det C$, and the scalar g, which satisfies $g^2 = 1 - \det C$ [12].

We now transform the injected beam matrix $\tilde{\sigma}$, which is given in physical coordinates to the coordinates of normalized phase space in the ring, which we call σ. Analogously to what we did in Eq. (48), we transform it with $\mathcal{A}$, which has the same structure as $\tilde{\mathcal{A}}$ from Eq. (51) but contains the Twiss parameters at the injection point of the ring. We then obtain

$$\begin{aligned} \sigma = \mathcal{A}\tilde{\sigma}\mathcal{A}^\top &= \mathcal{A}T^{-1}\tilde{\mathcal{A}}^{-1}\bar{\varepsilon}(\tilde{\mathcal{A}}^{-1})^\top (T^{-1})^\top \mathcal{A}^\top \\ &= \mathcal{A}T^{-1}\tilde{\mathcal{A}}^{-1}\bar{\varepsilon}(\mathcal{A}T^{-1}\tilde{\mathcal{A}}^{-1})^\top. \end{aligned} \tag{53}$$

Let us first calculate

$$K = \mathcal{A}T^{-1}\tilde{\mathcal{A}}^{-1} = \begin{pmatrix} g\mathcal{A}_x\tilde{\mathcal{A}}_a^{-1} & \mathcal{A}_x C\tilde{\mathcal{A}}_b^{-1} \\ -\mathcal{A}_y C^+\tilde{\mathcal{A}}_a^{-1} & g\mathcal{A}_y\tilde{\mathcal{A}}_b^{-1} \end{pmatrix}, \tag{54}$$

which we use to calculate $\sigma = K\bar{\varepsilon}K^\top$ and find the top-left 2×2 submatrix of σ to be

$$\begin{aligned} \begin{pmatrix} \sigma_{11} & \sigma_{12} \\ \sigma_{12} & \sigma_{22} \end{pmatrix} &= g^2\varepsilon_a\mathcal{A}_x\tilde{\mathcal{A}}_a^{-1}(\mathcal{A}_x\tilde{\mathcal{A}}_a^{-1})^\top \\ &\quad + \varepsilon_b\mathcal{A}_x C\tilde{\mathcal{A}}_b^{-1}(\mathcal{A}_x C\tilde{\mathcal{A}}_b^{-1})^\top, \end{aligned} \tag{55}$$

from which we calculate the asymptotically achievable emittance with $(\sigma_{11}+\sigma_{22})/2$, just as we did in the previous section. The lower-right submatrix contains a similar expression that describes the vertical plane from which we can calculate the asymptotically achievable vertical emittance $(\sigma_{33}+\sigma_{44})/2$.

We now consider the special case where C stems from a coordinate rotation with angle η. This leads to $g=\cos\eta$ and $C=-\mathbf{1}\sin\eta$. Inserting g and C into Eq. (55), we obtain

$$\begin{pmatrix}\sigma_{11} & \sigma_{12}\\ \sigma_{12} & \sigma_{22}\end{pmatrix} = \varepsilon_a\mathcal{A}_x\tilde{\mathcal{A}}_a^{-1}(\mathcal{A}_x\tilde{\mathcal{A}}_a^{-1})^\top\cos^2(\eta) + \varepsilon_b\mathcal{A}_x\tilde{\mathcal{A}}_b^{-1}(\mathcal{A}_x\tilde{\mathcal{A}}_b^{-1})^\top\sin^2(\eta). \tag{56}$$

The combination of matrices in the second term evaluates to

$$\mathcal{A}_x\tilde{\mathcal{A}}_b^{-1}(\mathcal{A}_x\tilde{\mathcal{A}}_b^{-1})^\top = \begin{pmatrix}\frac{\beta_b}{\beta_x} & \frac{\alpha_x\beta_b}{\beta_x}-\alpha_b\\ \frac{\alpha_x\beta_b}{\beta_x}-\alpha_b & \frac{\alpha_x^2\beta_b}{\beta_x}-2\alpha_x\alpha_b+\frac{1+\alpha_b^2}{\beta_b}\beta_x\end{pmatrix} \tag{57}$$

and to a similar expression for the first term after replacing β_b and α_b by β_a and α_a, respectively. From the sum of the diagonal elements, we obtain for the asymptotically achievable emittances in the horizontal and the vertical plane

$$\begin{aligned}\frac{1}{2}(\sigma_{11}+\sigma_{22}) &= \varepsilon_a\cos^2(\eta)B_{mag}(\beta_x,\beta_a)+\varepsilon_b\sin^2(\eta)B_{mag}(\beta_x,\beta_b),\\ \frac{1}{2}(\sigma_{33}+\sigma_{44}) &= \varepsilon_b\cos^2(\eta)B_{mag}(\beta_y,\beta_b)+\varepsilon_a\sin^2(\eta)B_{mag}(\beta_y,\beta_a)\\ \text{with}\quad B_{mag}(\beta_x,\beta_b) &= \frac{1}{2}\left[\left(\frac{\beta_x}{\beta_b}+\frac{\beta_b}{\beta_x}\right)+\beta_x\beta_b\left(\frac{\alpha_x}{\beta_x}-\frac{\alpha_b}{\beta_b}\right)^2\right],\end{aligned} \tag{58}$$

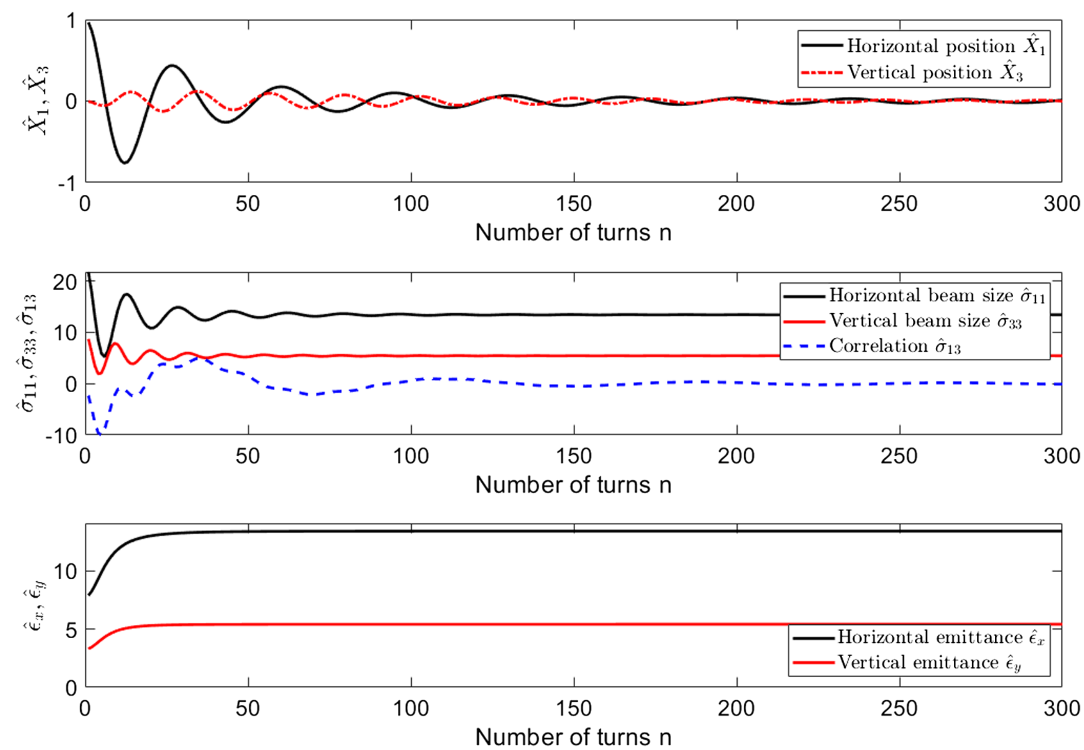

FIG. 5. The horizontal and vertical beam positions $\hat{X}_1$ and $\hat{X}_3$ (top), beam matrix elements (middle), and emittance (bottom) as a function of the number of turns for a beam with initial emittance ratio $\varepsilon_a/\varepsilon_b=10$, initial beta mismatch, and displacement. The beam is rotated by $\eta=30°$. The initial mismatch decoheres, and the emittance reaches its asymptotic value, given by Eq. (59).

where we do not write out the dependence on α_x and α_b in the definition of B_{mag}, whose definition from Eq. (49) is repeated here for convenience. In Eq. (58), it contains different combinations of horizontal and vertical Twiss parameters of the injected beam and those at the point of injection into the ring. It describes the influence of the Twiss parameters on the decoherence, which is smallest ($B_{mag} = 1$) if the Twiss parameters in the horizontal and vertical plane of the injection line and the ring are equal. Summarily, the asymptotic emittance growth, including the effect of initial displacement, in the horizontal plane then turns out to be

$$\hat{\varepsilon}_x = \varepsilon_a B_{mag}(\beta_x, \beta_a)\cos^2(\eta) + \varepsilon_b B_{mag}(\beta_x, \beta_b)\sin^2(\eta) + \frac{1}{2}(X_1^2 + X_2^2) \tag{59}$$

and a corresponding equation for the vertical emittance.

Figure 5 shows the turn-by-turn evolution of a beam with initial emittance ratio of $\varepsilon_a/\varepsilon_b = 10$ that is coupled by a coordinate rotation with $\eta = 30°$. The Twiss parameters of the injected beam are $\beta_a = \beta_b = 3$ m, and $\alpha_a = \alpha_b = 0$, which makes $B_{mag}(\beta_x, \beta_a) = B_{mag}(\beta_x, \beta_b) = 5/3$. Moreover, the beam is injected with an initial offset $X_1 = 1$. The tunes are 0.028 in the horizontal and 0.041 in the vertical plane, and the detuning parameters are $\kappa_{xx} = 10^{-3}$, $\kappa_{yy} = 2\times10^{-3}$, and $\kappa_{xy} = 5\times10^{-4}$. We observe in the upper panel that the beam initially performs horizontal betatron oscillations with decreasing amplitude, but the coupled beam matrix also causes the vertical centroid $\hat{X}_3$ to oscillate. Likewise, the horizontal and vertical beam sizes, both shown in the middle panel, initially oscillate but rapidly decohere, before settling on their equilibrium value. The correlation $\hat{\sigma}_{13}$, derived in the Appendix, shows a more complicated pattern, because it oscillates with the sum and difference frequency of the horizontal and vertical tune before also reaching its equilibrium value zero. The bottom panel shows the horizontal and vertical emittances increasing from their initial value, which is given by the projected emittance of the coupled beam at injection. Decoherence causes the emittances to asymptotically reach $\hat{\varepsilon}_x = 13.4$ and $\hat{\varepsilon}_y = 5.41$, consistent with the values calculated from Eq. (59).

VIII. DISPERSION

In this section, we consider the asymptotic emittance growth due to a mismatched and potentially coupled dispersion with $d = 4$. Here, we treat dispersion errors $\vec{D}$ as a momentum-dependent offset of the centroid, such that we just replace $\hat{X}$ by $\vec{D}\delta$ in Eq. (44). Subsequently, averaging over δ gives us the emittance growth as

$$\Delta\hat{\varepsilon} = \frac{1}{2}(D_1^2 + D_2^2)\sigma_\delta^2, \tag{60}$$

where σ_δ is the relative momentum spread in the ring. The dispersion errors $\vec{D}$ in normalized phase space are given by

$$\vec{D} = (D_1, D_2, D_3, D_4)^\top = \mathcal{A}T\begin{pmatrix}\vec{D}_x \\ \vec{D}_y\end{pmatrix} = \begin{pmatrix} g\mathcal{A}_x\vec{D}_x - \mathcal{A}_x C\vec{D}_y \\ \mathcal{A}_y C^+\vec{D}_x + g\mathcal{A}_y\vec{D}_y\end{pmatrix}, \tag{61}$$

where $\mathcal{A}$ from Eq. (51) contains the Twiss parameters and T from Eq. (52) describes transverse coupling. These two matrices transform the physical dispersions $\vec{D}_x = (D_x, D'_x)^\top$ and $\vec{D}_y = (D_y, D'_y)^\top$ in the horizontal and vertical plane of the transfer line into the normalized phase space of the ring. Evaluating $D_1^2 + D_2^2$ then leads to

$$D_1^2 + D_2^2 = g^2\vec{D}_x^\top\mathcal{A}_x^\top\mathcal{A}_x\vec{D}_x - 2g\vec{D}_y^\top C^\top\mathcal{A}_x^\top\mathcal{A}_x\vec{D}_x + \vec{D}_y^\top C^\top\mathcal{A}_x^\top\mathcal{A}_x C\vec{D}_y \tag{62}$$

and a similar expression for $D_3^2 + D_4^2$ that describes the emittance growth in the vertical plane. Equation (62) is valid for any coupling matrix C, but if we specifically evaluate it for a coordinate rotation with $g = \cos\eta$ and $C = -\mathbf{1}\sin\eta$, we find

$$D_1^2 + D_2^2 = \cos^2(\eta)\mathcal{H}_x(\vec{D}_x, \vec{D}_x) + 2\sin(\eta)\cos(\eta)\mathcal{H}_x(\vec{D}_y, \vec{D}_x) + \sin^2(\eta)\mathcal{H}_x(\vec{D}_y, \vec{D}_y), \tag{63}$$

where

$$\mathcal{H}_x(\vec{D}_y, \vec{D}_x) = \gamma_x D_x D_y + \alpha_x(D_y D'_x + D'_y D_x) + \beta_x D'_x D'_y \tag{64}$$

is the generalization of the quantity $\mathcal{H}_x$ that appears in the fifth radiation integral [13,14].

For $\eta = 0$, Eq. (63) characterizes the emittance growth due to a dispersion error $\vec{D}_x$ in the horizontal plane. The emittance growth then turns out to be

$$\Delta\hat{\varepsilon} = \frac{1}{2}\mathcal{H}_x(\vec{D}_x, \vec{D}_x)\sigma_\delta^2 = \frac{1}{2}(\gamma_x D_x^2 + 2\alpha_x D_x D'_x + \beta_x D'^2_x)\sigma_\delta^2, \tag{65}$$

which agrees with the expression derived in Ref. [15].

IX. CHROMATICITY

The decoherence of an unbunched beam with rms momentum spread σ_δ and a finite chromaticity Q' can be included in our framework by adding $\mu'_x\delta = 2\pi Q'_x\delta$ to the phase advance per turn ϕ_x from Eq. (1). This gives us

$$\phi_x = \mu_x + \vec{x}^\top \bar{\kappa}_x \vec{x} + \mu_x' \delta \quad \text{with} \quad \psi(\delta) = \frac{1}{\sqrt{2\pi}\sigma_\delta} e^{-\delta^2/2\sigma_\delta^2}. \tag{66}$$

Instead of just averaging over the transverse phase-space coordinates in Eq. (5), we now also have to average over the momentum δ with distribution $\psi(\delta)$. The integral factorizes into one part that depends on x_1 and x_2 and a second, momentum-dependent part $D(n)$, given by

$$D(n) = \int e^{-in\mu_x'\delta} e^{-\delta^2/2\sigma_\delta^2} d\delta = e^{-\mu_x'^2\sigma_\delta^2 n^2/2}, \tag{67}$$

which multiplies all integrals $I[n, \vec{p}]$.

For bunched beams that perform synchrotron oscillations with frequency ν_s, the betatron phase advance after n turns is given by [1,4]

$$n\phi_x = n\mu_x + n\vec{x}^\top \bar{\kappa}_x \vec{x} + \zeta(n) \quad \text{with}$$
$$\zeta(n) = \frac{\mu_x'\delta}{\pi\nu_s} \sin(\pi\nu_s n)\cos(\pi\nu_s n + \eta_0), \tag{68}$$

where η_0 is the initial phase of the synchrotron oscillations. Averaging over η_0 and δ with the momentum distribution from Eq. (66) results in the form factor [1,4]

$$D(n) = \exp\left[-2\left(\frac{\mu_x'\sigma_\delta}{2\pi\nu_s}\right)^2 \sin^2(\pi\nu_s n)\right] \tag{69}$$

The form factor $D(n)$, either from Eq. (67) for unbunched beams or from Eq. (69) for bunched beams, becomes a multiplicative factor for $I[n, \vec{p}]$ that carries through all the way to Eq. (18), where it modulates the right-hand side. In the same fashion, all $J[-2n, x_r x_2]$ in Eqs. (29), (A2), and (A5) assume an additional factor $D(n)^4$, because the step from n to $2n$ doubles $\zeta(n)$, which is equivalent to doubling μ_x' that causes the exponent of $D(n)$ to quadruple. Apart from these additional factors, all other equations remain unchanged. In particular, the asymptotic equilibrium values of the beam matrix and the emittance, which are multiplied by powers of $D(0) = 1$, from Eqs. (50) and (58) remain unaffected. Only the temporal evolution toward equilibrium is modulated by the powers of $D(n)$ which prepend the $J(\pm 2n, x_r x_s)$.

X. TOLERANCES

Here, we analyze the requirements for the steering errors and the Twiss parameters of an injected beam to cause an emittance growth of less than 1% and 5%. To do so, we expand Eq. (50) up to second order in the deviations from their respective design values $\Delta\beta = \beta_0 - \beta$, $\Delta\alpha = \alpha_0 - \alpha$, ΔX, and $\Delta X'$ and find for the asymptotic emittance increase

TABLE I. The tolerance levels for mismatch and steering errors for the injection into the SPS. The nominal emittance is $\varepsilon_0 = 1.26 \times 10^{-7}$ m rad, and the Twiss parameters at the injection point are $\beta = 44.5$ m and $\alpha = -0.96$.

Tolerance level	$\Delta\beta/\beta$	$\Delta\alpha$	ΔX [mm]	$\Delta X'$ [μrad]
1%	0.14	0.14	0.24	7.5
5%	0.32	0.32	0.54	16.8

$$\hat{\varepsilon} - \varepsilon_0 = \frac{1}{2}\left(\frac{\Delta\beta}{\beta}\right)^2 + \frac{1}{2}\Delta\alpha^2 + \frac{\gamma}{2}\Delta X^2 + \frac{\beta}{2}\Delta X'^2 \tag{70}$$

with $\gamma = (1 + \alpha^2)/\beta$. As an example, we use the horizontal injection from the TT10 transfer line into the Super Proton Synchrotron (SPS) [16] when it serves beams to the LHC. In this configuration, the horizontal Twiss parameters [17] at the injection point are $\beta = 44.5$ m and $\alpha = -0.96$. Moreover, the emittance is $\varepsilon_0 = 1.26 \times 10^{-7}$ m rad. The tolerance levels that increase the asymptotic emittance by 1% and 5% are shown in Table I. We find that the error tolerances for the Twiss parameters are fairly relaxed; even errors of $\Delta\beta/\beta$ or $\Delta\alpha$ in the 10% range increase the emittance by less than 1%. On the other hand, owing to the relatively large value of β at the injection point, steering errors $\Delta X'$ exceeding 20 μrad lead to increased emittances above the 5% level.

XI. CONCLUSION

We derived evolution equations for the first and second moments of an coupled arbitrary Gaussian phase-space distribution that initially is mismatched and displaced and has mismatched dispersion under the influence of decoherence due to amplitude-dependent tune shift. The well-known results from Refs. [1,4] for the amplitude dependence of the first and second moments after an initial displacement of a matched beam are reproduced. Our results go beyond Refs. [1,4], because the initial beam can have an arbitrary Gaussian distribution, which includes transverse coupling, and does not need to be matched. We then calculate the temporal evolution of the second moments, the beam sizes, and the emittance. Moreover, we calculate the emittance in the asymptotic limit and find it to agree with the emittance growth due to chromatic effects. Finally, we analyzed tolerances for the injection and used the SPS as an illustration.

ACKNOWLEDGMENTS

We acknowledge financial support from Uppsala University (V. Z.) and from CERN (E. W.). We gratefully acknowledge discussions with Francesco Velotti and the hospitality of the ABT group at CERN.

APPENDIX: SECOND MOMENTS

In Eq. (27), we show only one of the second-order moments. The other two that are needed for the horizontal plane are calculated in a similar fashion from

$$\begin{aligned}\langle\hat{x}_1\hat{x}_2\rangle &= \langle(x_1\cos n\phi_x + x_2\sin n\phi_x)(-x_1\sin n\phi + x_2\cos n\phi)\rangle,\\ \langle\hat{x}_2^2\rangle &= \langle(-x_1\sin n\phi_x + x_2\cos n\phi_x)^2\rangle,\end{aligned} \tag{A1}$$

where the angle brackets denote averaging over the Gaussian from Eq. (3) in d dimensions. Following steps similar to those leading to Eq. (29) brings us to

$$\begin{aligned}\langle\hat{x}_1^2\rangle &= \frac{1}{4}(2J[0,x_1^2] + J[-2n,x_1^2] + J[2n,x_1^2]) - \frac{i}{2}(J[-2n,x_1x_2] - J[2n,x_1x_2])\\ &\quad + \frac{1}{4}(2J[0,x_2^2] - J[-2n,x_2^2] - J[2n,x_2^2]),\\ \langle\hat{x}_1\hat{x}_2\rangle &= -\frac{1}{4i}(J[-2n,x_1^2] - J[2n,x_1^2]) + \frac{1}{2}(J[-2n,x_1x_2] + J[2n,x_1x_2])\\ &\quad + \frac{1}{4i}(J[-2n,x_2^2] - J[2n,x_2^2]),\\ \langle\hat{x}_2^2\rangle &= \frac{1}{4}(2J[0,x_1^2] - J[-2n,x_1^2] - J[2n,x_1^2]) + \frac{i}{2}(J[-2n,x_1x_2] - J[2n,x_1x_2])\\ &\quad + \frac{1}{4}(2J[0,x_2^2] + J[-2n,x_2^2] + J[2n,x_2^2]),\end{aligned} \tag{A2}$$

where, for completeness, we also show the expression for $\langle\hat{x}_1^2\rangle$ from Eq. (29). We can simplify these expressions further by noting that

$$J[-m,p] + J[m,p] = \langle e^{im\phi_x}p\rangle + \langle e^{-im\phi_x}p\rangle = 2\mathrm{Re}\langle e^{im\phi_x}p\rangle = 2\mathrm{Re}(J[-m,p]) \tag{A3}$$

and likewise

$$J[-m,p] - J[m,p] = 2i\mathrm{Im}(J[-m,p]), \tag{A4}$$

which allows us to write

$$\begin{aligned}\langle\hat{x}_1^2\rangle &= \frac{1}{2}\{J[0,x_1^2] + \mathrm{Re}(J[-2n,x_1^2])\} + \mathrm{Im}(J[-2n,x_1x_2]) + \frac{1}{2}\{J[0,x_2^2] - \mathrm{Re}(J[-2n,x_2^2])\},\\ \langle\hat{x}_1\hat{x}_2\rangle &= -\frac{1}{2}\mathrm{Im}(J[-2n,x_1^2]) + \mathrm{Re}(J[-2n,x_1x_2]) + \frac{1}{2}\mathrm{Im}(J[-2n,x_2^2]),\\ \langle\hat{x}_2^2\rangle &= \frac{1}{2}\{J[0,x_1^2] - \mathrm{Re}(J[-2n,x_1^2])\} - \mathrm{Im}(J[-2n,x_1x_2]) + \frac{1}{2}\{J[0,x_2^2] + \mathrm{Re}(J[-2n,x_2^2])\}.\end{aligned} \tag{A5}$$

The second moments of the type $\langle\hat{x}_1\hat{x}_3\rangle$ arise if we consider coupled motion and need special attention, because $\hat{x}_1$ oscillates with μ_x and $\hat{x}_3$ with μ_y. Likewise, the amplitude-dependent tune shift in the horizontal plane is given by $\vec{x}^\top\bar{\kappa}_x\vec{x}$ and by $\vec{x}^\top\bar{\kappa}_y\vec{x}$ with $\bar{\kappa}_y = \mathrm{diag}(\kappa_{xy},\kappa_{xy},\kappa_{yy},\kappa_{yy})$ in the vertical plane. Since we will encounter $J[m,p;\mu_x,\bar{\kappa}_x]$ from Eq. (28) for different arguments μ_x and $\bar{\kappa}_x$, we specify all arguments henceforth when we calculate $\langle\hat{x}_1\hat{x}_3\rangle$ for which we find

$$\begin{aligned}
\langle\hat{x}_1\hat{x}_3\rangle &= \langle[x_1\cos(n\phi_x)+x_2\sin(n\phi_x)][x_3\cos(n\phi_y)+x_4\sin(n\phi_y)]\rangle \\
&= \frac{1}{4}\langle x_1x_3[e^{in(\phi_x+\phi_y)}+e^{in(\phi_x-\phi_y)}+e^{-in(\phi_x-\phi_y)}+e^{-in(\phi_x+\phi_y)}]\rangle \\
&\quad+\frac{1}{4i}\langle x_1x_4[e^{in(\phi_x+\phi_y)}-e^{in(\phi_x-\phi_y)}+e^{-in(\phi_x-\phi_y)}-e^{-in(\phi_x+\phi_y)}]\rangle \\
&\quad+\frac{1}{4i}\langle x_2x_3[e^{in(\phi_x+\phi_y)}+e^{in(\phi_x-\phi_y)}-e^{-in(\phi_x-\phi_y)}-e^{-in(\phi_x+\phi_y)}]\rangle \\
&\quad-\frac{1}{4}\langle x_2x_4[e^{in(\phi_x+\phi_y)}-e^{in(\phi_x-\phi_y)}-e^{-in(\phi_x-\phi_y)}+e^{-in(\phi_x+\phi_y)}]\rangle \\
&= \frac{1}{4}\{2\mathrm{Re}(J[-n,x_1x_3;\mu_x+\mu_y,\bar{\kappa}_x+\bar{\kappa}_y])+2\mathrm{Re}(J[-n,x_1x_3;\mu_x-\mu_y,\bar{\kappa}_x-\bar{\kappa}_y])\} \\
&\quad+\frac{1}{4i}\{2i\mathrm{Im}(J[-n,x_1x_4;\mu_x+\mu_y,\bar{\kappa}_x+\bar{\kappa}_y])-2i\mathrm{Im}(J[-n,x_1x_4;\mu_x-\mu_y,\bar{\kappa}_x-\bar{\kappa}_y])\} \\
&\quad+\frac{1}{4i}\{2i\mathrm{Im}(J[-n,x_2x_3;\mu_x+\mu_y,\bar{\kappa}_x+\bar{\kappa}_y])+2i\mathrm{Im}(J[-n,x_2x_3;\mu_x-\mu_y,\bar{\kappa}_x-\bar{\kappa}_y])\} \\
&\quad-\frac{1}{4}\{2\mathrm{Re}(J[-n,x_2x_4;\mu_x+\mu_y,\bar{\kappa}_x+\bar{\kappa}_y])-2\mathrm{Re}(J[-n,x_2x_4;\mu_x-\mu_y,\bar{\kappa}_x-\bar{\kappa}_y])\}.
\end{aligned} \tag{A6}$$

The last equality is a sum of terms very much like those from Eq. (29). Only here the phase advance μ_x is replaced by $\mu_x \pm \mu_y$ and $\bar{\kappa}_x$ by $\bar{\kappa}_x \pm \bar{\kappa}_y$. We can, therefore, use the same MATLAB function for $J[m,p;\mu_x,\bar{\kappa}_x]$ to work out $\langle\hat{x}_1\hat{x}_3\rangle$ and determine $\hat{\sigma}_{13} = \langle\hat{x}_1\hat{x}_3\rangle - \hat{X}_1\hat{X}_3$ shown on the middle panel in Fig. 5.

[1] R. Meller, A. Chao, J. Peterson, S. Peggs, and M. Furman, Decoherence of kicked beams, Report No. SSC-N-360, 1987.

[2] S. Y. Lee, Decoherence of the kicked beams II, Report No. SSC-N-749, 1991.

[3] A. Sargsyan, Transverse decoherence of the kicked beams due to amplitude and chromaticity tune shifts, Nucl. Instrum. Methods Phys. Res., Sect. A **638**, 15 (2011).

[4] M. Minty, A. Chao, and W. Spence, in *Proceedings of the Particle Accelerator Conference, Dallas, TX, 1995* (IEEE, New York, 1995), p. 3037, 10.1109/PAC.1995.505776.

[5] M. Furman, in *Handbook of Accelerator Physics and Engineering*, 1st ed. (World Scientific, Singapore, 1999), Sec. 2.3.10.

[6] A. Verdier, Cross anharmonicity, AIP Conf. Proc. **344**, 269 (1995).

[7] J. Zinn-Justin, *Quantum Field Theory and Critical Phenomena*, 4th ed. (Clarendon, Oxford, 2002), Sec. 1.1.

[8] MATLAB Web page: https://www.mathworks.com.

[9] Github repository with the software for the simulations: https://github.com/volkziem/InjectionDecoherence.

[10] V. Ziemann, *Hands-On Accelerator Physics Using MATLAB* (CRC Press, Boca Raton, 2019).

[11] D. Edward and L. Teng, Parametrization of linear coupled motion in periodic systems, IEEE Trans. Nucl. Sci. **20**, 885 (1973).

[12] D. Sagan and D. Rubin, Linear analysis of coupled lattices, Phys. Rev. Accel. Beams **2**, 074001 (1999).

[13] R. Helm, M. Lee, and P. Morton, Evaluation of synchrotron radiation integrals, IEEE Trans. Nucl. Sci. **20**, 900 (1973).

[14] V. Ziemann and A. Streun, Equilibrium parameters in coupled storage ring lattices and practical applications, Phys. Rev. Accel. Beams **25**, 050703 (2022).

[15] G. Arduini and P. Raimondi, Transverse emittance blow-up due to injection errors, CERN Report No. SL-Note-99-022, 1999.

[16] P. Collier *et al.*, SPS as injector for LHC: Conceptual design report, Report No. CERN SL-97-07 DI, CERN, 1997.

[17] CERN optics repository, Q20 optics function for SPS injection, available at https://acc-models.web.cern.ch/acc-models/tls/2021/sps_injection/tt2tt10_lhc_q20/stitched/.